

# Effects of spin vacancies on magnetic properties of the Kitaev-Heisenberg model

Fabien Trouselet, Giniyat Khaliullin, and Peter Horsch

Max-Planck-Institut für Festkörperforschung, Heisenbergstrasse 1, D-70569 Stuttgart, Germany

(Dated: March 3, 2018)

We study the ground state properties of the Kitaev-Heisenberg model in a magnetic field and explore the evolution of spin correlations in the presence of non-magnetic vacancies. By means of exact diagonalizations, the phase diagram without vacancies is determined as a function of the magnetic field and the ratio between Kitaev and Heisenberg interactions. We show that in the (antiferromagnetic) stripe ordered phase the static susceptibility and its anisotropy can be described by a spin canting mechanism. This accounts as well for the transition to the polarized phase when including quantum fluctuations perturbatively. Effects of spin vacancies depend sensitively on the type of the ground state. In the liquid phase, the magnetization pattern around a single vacancy in a small field is determined, and its spatial anisotropy is related to that of *non-zero* further neighbor correlations induced by the field and/or Heisenberg interactions. In the stripe phase, the joint effect of a vacancy and a small field breaks the six-fold symmetry of the model and stabilizes a particular stripe pattern. Similar symmetry-breaking effects occur even at zero field due to effective interactions between vacancies. This selection mechanism and intrinsic randomness of vacancy positions may lead to spin-glass behavior.

PACS numbers: 75.10.Jm, 75.30.Et, 71.55.-i, 71.30.+h

## I. INTRODUCTION

Much attention has been paid recently to the existence and properties of spin liquids in strongly correlated materials, both experimentally and theoretically<sup>1,2</sup>. Such phases, first proposed by Anderson, have been put forward in the context of high  $T_c$  superconductivity as a possible precursor state, but they can occur in a much broader class of situations, both in real materials<sup>3-6</sup> and in microscopic models<sup>7-10</sup>. Their characterization is challenging – on the experimental side, it requires generally involved low-temperature techniques to prove the absence of long-range magnetic order down to temperature  $T = 0$ , and concerning the theory, either in Hubbard-like models or in localized spin models, spin liquids usually result from frustrating interactions but compete with a variety of possible ordered phases, from usual antiferromagnetic (AF) order to valence bond crystals, spin nematics etc.<sup>2</sup>

Clear evidence of a spin liquid ground state was found from an exact solution of the Kitaev model<sup>11</sup> of spins  $1/2$  on the honeycomb lattice. This liquid ground state is characterized by a gapless spectrum (with low-energy excitations described in terms of Majorana fermions) and gapped vortices. The Kitaev model itself triggered a large variety of studies, focusing on topological properties, (non)-abelian excitations, extensions to higher dimensions<sup>12</sup>, effects of magnetic<sup>13</sup> or non-magnetic impurities and of a magnetic field<sup>11,14-16</sup>.

Besides its mathematical beauty and the original properties mentioned above, the Kitaev model was recently found<sup>17</sup> to be relevant to orbitally degenerate systems with strong spin-orbit coupling such as layered iridates  $\text{Na}_2\text{IrO}_3$  and  $\text{Li}_2\text{IrO}_3$ . There, around each Ir atom, the octahedral environment [see Fig. 1(a)] of oxygens results in a configuration with one hole in the  $t_{2g}$  manifold;

and the large spin-orbit coupling selects locally a low-energy doublet of states defining a pseudospin  $1/2$ ; and finally, superexchange processes between Ir ions driven by moderately strong Coulomb interactions lead to an effective description by the Kitaev-Heisenberg model<sup>17,18</sup> for pseudospins  $1/2$  residing on the honeycomb lattice. The study of this model showed the robustness of the spin liquid phase for finite AF Heisenberg interactions [small compared to ferromagnetic (FM) Kitaev interactions], and a quantum phase transition between this liquid phase and a stripe-ordered phase. In  $\text{Na}_2\text{IrO}_3$ , where interaction parameters could be close to this transition, AF order was found by magnetization and specific heat measurements<sup>19,20</sup> and x-ray magnetic scattering<sup>21</sup>.

The question of how vacancies influence the order and the magnetic response in the Kitaev-Heisenberg model is of both experimental and theoretical interest. Indeed the vacancy can act as a probe allowing to measure spin correlations in its vicinity; and it can also have drastic effects on these correlations. For concreteness, in  $SU(2)$  spin- $1/2$  antiferromagnets with long-range order, a non-magnetic impurity can enhance the staggered magnetization around the vacancy<sup>22,23</sup>. In dimerized phases, the impurity is accompanied by a spinon, which is typically confined to the impurity in Valence Bond Crystals and deconfined in Resonating Valence Bond liquids<sup>24</sup>, although the question of the confinement length can be subtle<sup>25</sup>. In a Néel-ordered phase, the impurity results in a Curie-type contribution to the finite- $T$  susceptibility<sup>26</sup>. In the spin-liquid phase of the Kitaev model, a magnetic moment is induced around a spinless vacancy; interestingly, its contribution to the spin susceptibility diverges logarithmically for  $T \rightarrow 0$ <sup>15</sup>. This makes it relevant to investigate the vacancy-induced magnetic response in a model interpolating between  $SU(2)$  and Kitaev-like interactions. Moreover, in the iridate samples studied up to

now, a substantial amount of disorder might be present, e.g., site-mixing effects with non-magnetic alkaline ions on the hexagonal Ir-sublattice<sup>20</sup>, which should be taken into account for proper understanding of their physical properties.

Our aim is to study the effect of non-magnetic vacancies (and of pairs of vacancies) in the different magnetic phases of the Kitaev-Heisenberg model, at zero temperature. We adopt similar notations as in Ref. 18, with a parameter  $0 \leq \alpha \leq 1$  interpolating between Heisenberg and Kitaev models, and a uniform magnetic field  $\vec{h} = (h_x, h_y, h_z)$  with amplitude  $h = \sqrt{h_x^2 + h_y^2 + h_z^2}$ :

$$H = -2\alpha \sum_{\langle i,j \rangle_\gamma} \sigma_i^\gamma \sigma_j^\gamma + (1-\alpha) \sum_{\langle i,j \rangle} \vec{\sigma}_i \cdot \vec{\sigma}_j - \sum_i \vec{h} \cdot \vec{\sigma}_i, \quad (1)$$

where  $\gamma = x, y, z$  labels simultaneously an axis in spin space, and (in the interaction terms) a bond direction of the honeycomb lattice. For convenience we express  $H$  in terms of Pauli matrices  $\vec{\sigma}_i$ . We take as unit cell a  $z$ -bond [see Fig. 1(b,c)], on which Kitaev interactions are of the form  $\sigma_i^z \sigma_j^z$ . Each site is labeled by an index  $i$ , in bijection with  $(\vec{r}, \beta)$  where  $\vec{r}$  denotes the position of the unit cell and  $\beta = A, B$  the sublattice index, respectively. Elementary translations between neighbor cells are  $\vec{n}_{1/2} = (\pm 1/2, \sqrt{3}/2)$  in Cartesian coordinates. We consider periodic clusters of  $N = 24$  sites (this cluster can be represented with an hexagonal shape, see Fig. 6),  $N = 32$  or  $N = 16$  sites (both with the shape of a parallelogram). These clusters respect all spatial symmetries of the model, i.e. translation and  $\pi$ -rotation - other symmetries combining spin- and spatial rotations<sup>28</sup> are not used here.

In Section II, we discuss several features of the model in a magnetic field. We will show how a spin canting mechanism allows one to understand the phase diagram for a field oriented along an easy axis, as well as to understand a directional anisotropy of the static susceptibility. Also the perturbations due to Heisenberg interactions and due to small magnetic fields on the spin correlation functions are explored. In Section III, we study the effect of a single non-magnetic vacancy in the system, in various phases of the model, and analyze the magnetization pattern in the vicinity of this vacancy in a small field. In Section IV, we discuss situations where two vacancies, close enough to each other, effectively interact. We focus mainly on the stripe phase and explain the underlying mechanism of local selection of an ordered pattern by a vacancy pair. Section V provides a short summary and some concluding discussions.

## II. VACANCY-FREE SYSTEM: SPIN CORRELATIONS, MAGNETIZATION, PHASE DIAGRAM

We first consider some basic properties of the Kitaev-Heisenberg model in a magnetic field, and study the mag-

netic response to a field oriented along different crystallographic directions. This comparison is important because of the symmetry of the model, which is clearly not  $SU(2)$  invariant due to the Kitaev interactions. In the context of iridates, this anisotropy is due to spin-orbit coupling which results in the easy spin axes  $x \parallel [100]$ ,  $y \parallel [010]$ ,  $z \parallel [001]$  [corresponding to the octahedral axes, see Fig. 1(a)], compared to the cubic diagonal  $[111]$  direction. The clearest anisotropic features are seen in the stripe-ordered phase, and we compare this situation to that of the Néel phase.

### A. The competing phases in a magnetic field

We first want to characterize the various phases found in a magnetic field. It is already known<sup>18</sup> that at zero field, the spin liquid phase extends from  $\alpha_{S/L} \simeq 0.80$  to  $\alpha = 1$  (the Kitaev limit); the stripe-ordered phase, with spins pointing either in  $x$ ,  $y$  or  $z$  direction [for the last case, the spatial structure, i.e.  $z$ -stripe pattern, is shown in Fig. 2(a)], is located between  $\alpha_{N/S} \simeq 0.40$  and  $\alpha_{S/L}$ ; and a Néel-ordered phase is found for  $0 \leq \alpha < \alpha_{N/S}$ . To determine whether these phases persist in a magnetic field and to understand the magnetic response of the system, one needs adapted structure factors which act as order parameters. For the Néel phase, it reads:

$$S_{N\acute{e}el} = \frac{1}{N^2} \sum_{\vec{r}, \vec{r}'} \nu_{\beta, \beta'} \langle \vec{\sigma}_{\vec{r}, \beta} \cdot \vec{\sigma}_{\vec{r}', \beta'} \rangle \quad (2)$$

with  $\nu_{\beta, \beta'}$  being 1 for  $\beta = \beta'$ , and  $-1$  otherwise; for the stripe-ordered phase, the structure factors corresponding to  $x$ - and  $z$ - stripe patterns are defined as follows:

$$S^x(\vec{Q}_x) = \frac{1}{N^2} \sum_{\vec{r}, \vec{r}', \beta, \beta'} e^{i\vec{Q}_x \cdot (\vec{r}' - \vec{r})} \nu_{\beta, \beta'} \langle \sigma_{\vec{r}, \beta}^x \sigma_{\vec{r}', \beta'}^x \rangle, \quad (3)$$

$$S^z(\vec{Q}_z) = \frac{1}{N^2} \sum_{\vec{r}, \vec{r}', \beta, \beta'} e^{i\vec{Q}_z \cdot (\vec{r}' - \vec{r})} \langle \sigma_{\vec{r}, \beta}^z \sigma_{\vec{r}', \beta'}^z \rangle, \quad (4)$$

with  $\vec{Q}_{x/y/z}$  shown in Fig. 1(d); for instance,  $\vec{Q}_z = (0, \frac{2\pi}{\sqrt{3}})$  which is equivalent to the more intuitive  $\vec{Q}'_z = (2\pi, 0)$  (but which is not in the first Brillouin zone). Both wave vectors account for a phase factor  $-1$  between neighboring unit cells separated by  $(\pm 1/2, \pm \sqrt{3}/2)$  in real space. These structure factors also evidence the symmetries spontaneously broken in each of the 6-fold degenerate ground states in the stripe phase: indeed at zero field, in addition to translational symmetries, the Hamiltonian possesses a  $\mathbb{Z}_2 * \mathbb{Z}_3$  symmetry -  $\mathbb{Z}_2$  standing for the  $\vec{\sigma}_i \rightarrow -\vec{\sigma}_i$  transformation and  $\mathbb{Z}_3$  (labeled as  $C_3^*$  in Ref. 28) for the invariance by a cyclic permutation of the  $x$ ,  $y$  and  $z$  spin components coupled to a spatial rotation by  $2\pi/3$ .

Both AF (Néel and stripe) ordered phases of the model persist under moderate fields, which tilt spins by an angle proportional to the small field amplitude (*canted Néel*

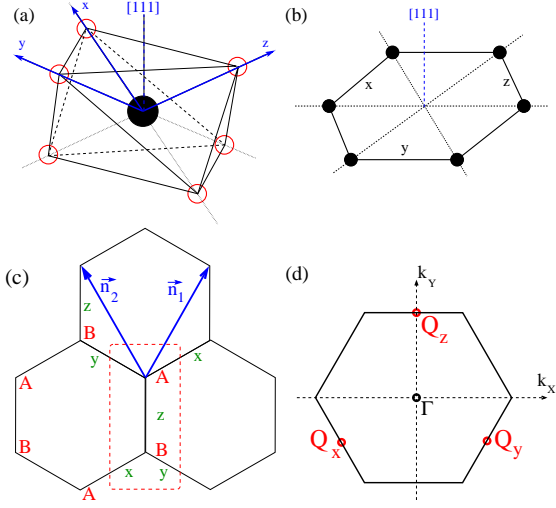


FIG. 1: (color online) (a) Schematic picture of an octahedron (6 oxygens surrounding a  $\text{Ir}^{4+}$  ion) with the octahedral axes  $x, y, z$  - which are easy axes on identically-labeled bonds in the Kitaev-Heisenberg model. (b) A hexagon in the  $\text{Ir}^{4+}$  plane, indicating bonds labeled  $x, y, z$  according to their local easy axis regarding Kitaev interactions. (c) Honeycomb (direct) lattice with the labeling  $x, y, z$  of bonds according to their in-plane orientation. A unit cell (centered on a  $z$ -bond) is represented in the dashed rectangle, as well as elementary translations  $\vec{n}_{1/2}$ . (d) First Brillouin zone, with the position of stripe-order wave vectors  $\vec{Q}_\gamma$  ( $\gamma = x, y, z$ ).

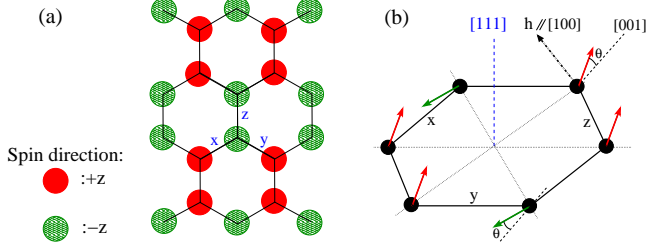


FIG. 2: (color online) (a) Representation of a  $z$ -stripe pattern (stripe pattern with spins oriented along the  $z = [001]$  axis - neighboring spins are aligned on  $z$  bonds and antialigned on other bonds). (b) Schematic representation, at the level of a single hexagon, of a canted stripe pattern: here a  $z$ -stripe pattern, with spins tilted of an angle  $\theta$  towards a field along  $[100]$  direction.

phase<sup>27</sup> or *canted stripe phase*<sup>28</sup>). To allow for this tilting, the untilted spins (for  $h$  infinitesimal) should not be collinear with the field<sup>30</sup>, and the staggered magnetization of the selected ordered pattern has an angle with  $\vec{h}$  as close to  $\pi/2$  as possible.

We first discuss the effect of a small field in the Néel phase, which allows to precise what we will understand in the following by (an)isotropy in the magnetic response. In the pure Heisenberg model, both classical and quantum cases, spontaneous breaking of  $SU(2)$  symmetry in

the thermodynamic limit leads to an anisotropic zero-field susceptibility. On the other hand, the ground state of a finite cluster is known to be a singlet, which does not break  $SU(2)$  symmetry. In order to perform a classical treatment of the Heisenberg model in absence of spontaneous symmetry breaking, one can consider for instance a  $SU(2)$  symmetric combination of classical Néel states - such a state can mimic, from an experimental viewpoint, the response of a polycrystalline sample. The magnetic response of this state is isotropic in the sense that a small field results in a magnetization of amplitude  $m_0$  along the field, and  $m_0$  does not depend on the field direction. When considering the Kitaev-Heisenberg model for small finite  $\alpha$ , with the classical approach above, one can find for any field direction a Néel pattern with spins perpendicular to it; within this approximation, the magnetic response is again isotropic, despite the absence of  $SU(2)$  symmetry due to small Kitaev interactions. However, the combination of quantum fluctuations and small Kitaev interactions have been found to select one of the cubic axes as an easy spin axis and open thereby a small spin gap<sup>18</sup>; this will lead to small anisotropies in the spin susceptibility.

In the stripe phase, even at the classical level only six ordered patterns are allowed at zero field. For a generic field  $\vec{h}$  with  $h_x, h_y$  and  $h_z$  taking three distinct values, the three allowed stripe orientations are energetically differentiated, depending on the field direction. For instance, in a small field  $h \parallel [100]$ , the two  $z$ -stripe patterns are favored (along with the  $y$ -stripe patterns), since they allow for the field to tilt spins by a small angle  $\theta$  [see Fig. 2(b)], such that the uniform magnetization develops an  $x$ -component. This effect is evidenced by structure factors characteristic of the ordered phase - in the case of Fig. 3 (with  $\alpha = 0.6$ ), in a small  $[001]$ -oriented field the  $x$ -stripe pattern becomes more favorable than the  $z$ -stripe pattern:  $S^x(\vec{Q}_x)$  jumps from approximately  $1/3$  at  $h = 0$  to  $1/2$  at small finite  $h_z$ , while  $S^z(\vec{Q}_z)$  (not shown) drops to almost 0. As for the magnetization per site  $m_0(h_z)$ , it grows linearly with  $h_z$  in this regime.

The tilting angle  $\theta$  can be determined simply in the classical approach, where the energy per unit cell as function of  $\theta$ , for given  $\alpha$  and  $h_z$ , is:

$$E_S(h_z, \theta) = -(1 + \alpha) - 2h_z \sin \theta + 4(1 - \alpha) \sin^2 \theta, \quad (5)$$

and its minimization w.r.t.  $\theta$  gives a magnetization per spin  $m_0 = \sin \theta_0 = \frac{h_z}{4(1-\alpha)}$ , in relatively good agreement with the linear behavior observed at small field (see Fig. 3 for the case  $\alpha = 0.6$ ); also, the predicted  $\alpha$ -dependence of the (uniform) susceptibility per spin,

$$\chi^z = \left( \frac{dm_0}{dh_z} \right)_{h=0} = \frac{1}{4(1-\alpha)}, \quad (6)$$

is in good agreement with the numerical results in Fig. 5. Note that the direction of the field is relevant in the stripe phase: a field  $h \parallel [001]$  differentiates stripe patterns,

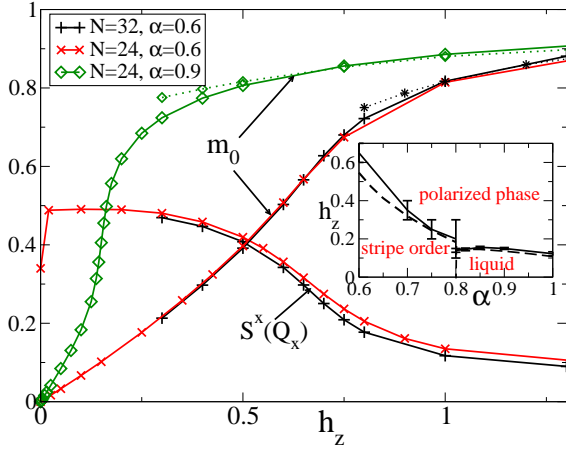


FIG. 3: (color online) Magnetization  $m_0$  (per site) and  $x$ -stripe structure factor  $S^x(\vec{Q}_x)$  versus  $h_z$  for various values of  $\alpha$  and  $N$ . Dotted lines: Perturbative results for  $m_0$  in the polarized phase. Inset: Phase diagram in the  $(\alpha, h_z)$  plane; continuous transition lines are interpolations of points from  $N = 24$  data and dashed lines are perturbative estimates.

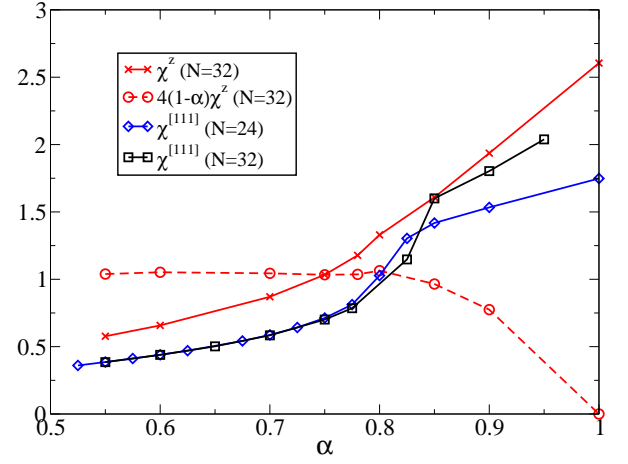


FIG. 5: (color online) Susceptibility per spin  $\chi^z$ , evaluated as  $m_0/h_z$  for small  $h_z = 0.01$ , and its equivalent  $\chi^{[111]}$  for a  $[111]$ -oriented field, on clusters  $N = 24$  or  $N = 32$ . Shown also the quantity  $4(1 - \alpha)\chi^z$  for  $N = 32$ .

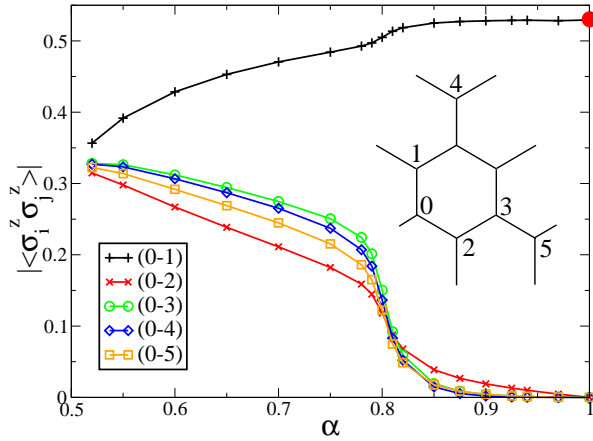


FIG. 4: (color online) Evolution of correlations  $|\langle \sigma_i^z \sigma_j^z \rangle|$  with  $\alpha$  on a  $N = 24$  cluster at  $h = 0$ , for various relative positions  $(i-j)$  with  $i$  and  $j$  indicated in the inset. The red dot indicates the value  $\sim 0.53$  of the  $(0-1)$  correlation at  $\alpha = 1$ , which coincides with an analytical result from Ref. 14.

and selects two of them where spins are exactly orthogonal to the field as  $h \rightarrow 0$ ; in contrast, in a  $h \parallel [111]$  field the three stripe directions remain equivalent (thus  $S^x(\vec{Q}_x) = S^z(\vec{Q}_z) \simeq 1/3$  for  $h \rightarrow 0$ ); also, none of the uncanted stripe patterns is orthogonal to a  $[111]$ -field, so the magnetic response for this field direction necessarily differs from the response to a  $[001]$ -field.

We now turn to the spin liquid regime, corresponding to the weakly perturbed Kitaev model, and describe the effect of perturbations to the system. Our main focus is on the  $\langle \sigma_i^z \sigma_j^z \rangle$  correlations. In the pure Kitaev model ( $\alpha = 1$ ,  $h = 0$ ), these correlations are non-zero only

when  $i, j$  are nearest neighbors on a  $z$ -bond<sup>11,14</sup>, where they take a value  $\langle \sigma_i^z \sigma_j^z \rangle_{z}^{(\alpha=1, h=0)} \simeq 0.53$  which we can see in Fig. 4 (the finite-size correction to this quantity, i.e. to the ground state energy, is negligible even for the  $N = 24$  sites cluster).

The gapless nature of excitations persists in a small axial field  $h_z$ ; in contrast, a  $[111]$ -oriented field opens a gap resulting in a topologically ordered phase<sup>11,28</sup>. Yet even in the first case, the field causes peculiar  $\langle \sigma_i^z \sigma_j^z \rangle$  correlations with spatial oscillations perpendicular to  $z$ -bonds and a power-law decaying envelope, as shown for  $\alpha = 1$  in Ref. 16. Some of these trends appear in the spin-spin correlations displayed in Fig. 6(a). Due to the small size, one cannot identify a power-law behavior; but one notices that correlations decrease with distance, much more slowly in the direction parallel to  $z$  bonds than in the direction perpendicular to them (i.e. parallel to  $\vec{n}_1 - \vec{n}_2$ ). Given the periodic boundary conditions on the  $N = 24$  lattice, this is in agreement with the period of three unit cells for spatial oscillations predicted in Ref. 16. The liquid phase is stable with respect to small Heisenberg interactions (for  $\alpha > \alpha_{S/L} \simeq 0.80$  at zero field<sup>18</sup>). These interactions induce correlations between further neighbors, of different type than those induced by a small field [compare Fig. 6(a) and (b)]. The spatial alternation of sign on Fig. 6(b) reminds of the  $z$ -stripe pattern, with the difference that here these correlations are short-ranged. A proof of this last point has been given in Ref. 29 for  $h = 0$ , and indeed absolute values  $|\langle \sigma^z \sigma^z \rangle|$  of correlations shown in Fig. 4 seem to decrease rapidly – possibly exponentially – with distance, at least in the spatial direction orthogonal to  $z$  bonds. On nearest neighbors, these correlations are proportional to  $1 - \alpha$  (not too close to  $\alpha_{S/L}$ ). With both perturbations at play, i.e. when both  $1 - \alpha$  and  $h_z$  are finite and small, their



effects should add up; therefore, and since the correlations induced by Heisenberg terms decay exponentially, one should observe a correlation pattern with a power-law tail as in the case of  $\alpha = 1, h_z \neq 0$ , but modulated as in a  $z$ -stripe pattern for short distances, at least for  $h_z^2 \ll 1 - \alpha$ .

Eventually, for any value of  $\alpha$ , a sufficiently high field drives the system into a *polarized phase* with spins parallel to  $\vec{h}$ . In the case of a [001]-field, by considering transverse interactions  $\sigma_i^x \sigma_j^x$  and  $\sigma_i^y \sigma_j^y$  as perturbations [the unperturbed ground state being fully polarized for  $h_z > 2(1 - \alpha)$ ], within second order perturbation theory one finds

$$m_0 = \langle \sigma_z \rangle \simeq 1 - \frac{\alpha^2}{(h_z + 4\alpha - 2)^2}, \quad (7)$$

in good agreement with numerical data for  $h_z \gtrsim 1$  (see dashed curves in Fig. 3).

### B. Transitions between liquid, stripe-ordered, and polarized phases

When a magnetic field  $h_z$  is applied to a system which is initially stripe- or Néel ordered, aside from the spin canting in the AF ordered state, the excitation energy of a competing polarized state decreases with  $h_z$  so that this state becomes the ground state above a critical field  $h_{S/F}$ . This field can be evaluated by estimating the energies (both per unit cell)  $E_S(h_z)$  of the canted stripe phase and  $E_{Fz}(h_z)$  of the polarized phase, as a function of field - then the equation  $E_S = E_{Fz}$  determines  $h_{S/F}$ . For both quantities, we add to the classical value a term (last terms in both lines of Eq. 8) accounting for quantum fluctuations, considered in second order perturbation theory, and evaluated respectively from the uncanted stripe- or the fully polarized state:

$$\begin{aligned} E_S(h_z) &= -(1 + \alpha) - \frac{1}{4} \frac{h_z^2}{1 - \alpha} - \frac{(1 - 2\alpha)^2}{\alpha}, \\ E_{Fz}(h_z) &= -2h_z + 3 - 5\alpha - \frac{2\alpha^2}{h_z + 4\alpha - 2}. \end{aligned} \quad (8)$$

We compare this estimate of  $h_{S/F}$  with numerical estimates obtained from the  $h_z$ -dependence of the stripe structure factor  $S^x(\vec{Q}_x)$  and the magnetization  $m_0$  for  $N = 24$  and  $N = 32$  clusters - both quantities show very weak size-dependence (see Fig. 3) and their derivatives with respect to  $h_z$  are maximized for values very close to each other. For  $\alpha = 0.6$ , this numerical estimation gives  $h_{S/F} = 0.65(5)$  compared to a value 0.55 found from the criterion  $E_S = E_{Fz}$ . Both types of estimates are shown as a function of  $\alpha$ , in the phase diagram in the inset of Fig. 3. For  $\alpha > \alpha_{S/L}$ , the magnetization curve  $m_0(h_z)$  on a finite cluster at fixed  $\alpha$  ( $\alpha = 0.9$  in Fig. 3) shows a sharp increase in a field range centered on  $h_{L/F} \simeq 0.15(1)$ ; this value is used to locate the transition to the polarized phase (our precision on  $h_{L/F}$  is limited

here by larger finite size effects in the liquid state than in ordered phases). This can be understood by modeling the energy per unit cell for the liquid phase by

$$E_L = 3(1 - 3\alpha) \langle \sigma^\gamma \sigma^\gamma \rangle_{\gamma}^{(\alpha=1, h=0)} - \chi^z h_z^2, \quad (9)$$

and looking for the field value such that  $E_L = E_{Fz}$ . This gives a value  $h_{L/F} \simeq 0.13(3)$ , which increases slightly with  $1 - \alpha$ . Similarly, the position of the stripe-liquid transition, which at zero field occurs at  $\alpha_{S/L}$ , is almost insensitive to a small field  $h_z$ .

The schematic phase diagram in Fig. 3 has a similar structure as its counterpart for a [111]-oriented field<sup>28</sup>, except that we do not see a multicritical point at  $\alpha = \alpha_{S/L}, h_z = 0$ . This may be connected with the absence of  $C_3^*$  symmetry in the Hamiltonian Eq. 1 in a [001]-field; moreover, the nature of the spin liquid for  $\alpha > \alpha_{S/L}$  in a small axial field differs from that of the topologically ordered phase in a small [111]-field, mainly in the structure of the low-energy spectrum.

### C. Susceptibility anisotropy

We analyze now in more detail the zero-field susceptibility: it has unusual properties due to a special spin symmetry of the model, which is lower than  $SU(2)$ . In the stripe phase ( $\alpha_{N/S} < \alpha < \alpha_{S/L}$ ), if we consider the general case of a  $[mnp]$ -oriented field, that is  $\vec{h}$  parallel to  $m\vec{x} + n\vec{y} + p\vec{z}$ , the corresponding susceptibility  $\chi^{[mnp]}$  behaves as  $\frac{c_{mnp}}{1 - \alpha}$ , where  $c_{mnp}$  is a rational number which can be found from the classical picture of a spin-flop mechanism. One can see in Fig. 5 that susceptibilities along different axes follow well this type of law in the stripe phase. The coefficient  $c_{mnp}$  is maximized for a [001]-field ( $c_{001} = 1/4$ , see Eq. 6), but also for a [101]-field, and minimized for a [111]-field ( $c_{111} = 1/6$ ). Note here that the [111] axis corresponds, in the context of susceptibility measurements in Ref. 20, to the  $c$  axis of  $\text{Na}_2\text{IrO}_3$ , i.e. perpendicular to the Ir-honeycomb layers [see Fig. 1(b)]. Concerning the susceptibility in the  $ab$  plane, this model predicts that - in the stripe phase -  $\chi$  takes a value between  $\chi^{[001]} = \frac{1}{4(1 - \alpha)}$  and  $\chi^{[112]} = \frac{1}{5(1 - \alpha)}$ . An average over the field orientations in the  $ab$  plane gives  $4(1 - \alpha) \langle \chi^{ab} \rangle = 2/3 + \frac{\sqrt{3}}{2\pi} \simeq 0.94$ .

No such simple expressions for the susceptibility are available for the liquid phase; but there, despite large finite-size effects (compared to the stripe phase) one notices that for a given axis susceptibilities tend to increase with  $\alpha$ , with again  $\chi^{[111]} \leq \chi^{[001]}$ . As for the Néel phase, a classical approach does not predict there any anisotropy in the static susceptibility (see related discussion in Section II A), and the anisotropy resulting from quantum fluctuations at small finite  $\alpha$  should be smaller than in the stripe phase - but the Néel phase is obtained for values of  $\alpha$  likely unrealistic for  $\text{Na}_2\text{IrO}_3$ <sup>18</sup> and also not supported by experiment<sup>21</sup>.

The experimental data of Ref. 20 reveal an anisotropy in the static susceptibility as well, but the measured susceptibility is significantly larger along the  $c$  axis than in the  $ab$  plane, in contrast to our model prediction  $\chi^c < \chi^{ab}$ . This suggests that other factors could contribute to the susceptibility anisotropy<sup>31</sup>. For instance, anisotropic contributions are expected to arise from the Van Vleck susceptibility  $\chi_{VV}^{(ab)} \neq \chi_{VV}^{(c)}$ , and also via the  $g$ -value anisotropy in the ground-state Kramers doublet, i.e.,  $g_{ab} \neq g_c$ , due to lattice distortions lowering the octahedral symmetry. These effects involve the inclusion of higher, excited spin-orbital, states.

Nevertheless, we believe that the Kitaev-Heisenberg model describes some characteristic features of layered iridates: for instance, recent susceptibility measurements<sup>32</sup> on polycrystals of  $\text{Li}_2\text{IrO}_3$  and of  $\text{Na}_2\text{IrO}_3$  showed that the zero-temperature susceptibility was about twice higher for the first (Li) compound than for the second. Assuming that both compounds can be described by the Kitaev-Heisenberg model and are in the stripe phase, the value of  $\alpha$  for the Li compound should be significantly larger than for the Na compound - probably  $\alpha_{\text{Li}} \geq 0.6$  if one compares the paramagnetic Curie temperatures of both compounds and follows theoretical results of Ref. 33. This is actually in agreement with the law  $\chi \propto \frac{1}{1-\alpha}$  which we find for any field direction (and thus for polycrystalline samples): since by assumption  $\alpha_{Na} \geq \alpha_{N/S} \simeq 0.4$ , the observed ratio<sup>32</sup>  $\chi(\text{Li})/\chi(\text{Na}) \simeq 2$  would imply  $\alpha_{\text{Li}} \geq 0.7$ . This suggests that the Li-compound is quite close to the stripe-liquid transition.

In the following, we shall confine our study to the Kitaev-Heisenberg model and explore the role of non-magnetic vacancies, unavoidably present in real compounds, and which, in general, can significantly alter the properties of frustrated magnetic systems<sup>4,34</sup>.

### III. COMBINED EFFECT OF A SINGLE VACANCY AND A MAGNETIC FIELD ON SPIN CORRELATIONS

We now study the effect of a single non-magnetic vacancy on the magnetic response of the system, especially at low-field. As previously, we will address separately the different phases of the model.

#### A. Anomalous magnetization around a vacancy in the liquid phase

We start by considering the liquid phase, and choose the field direction along the  $[001]$  axis, for which features characteristic of the Kitaev model are the clearest. First, we show that the combination of an infinitesimal field and a spin vacancy induces a peculiar magnetization pattern around the vacancy. The relevant quantity is the induced

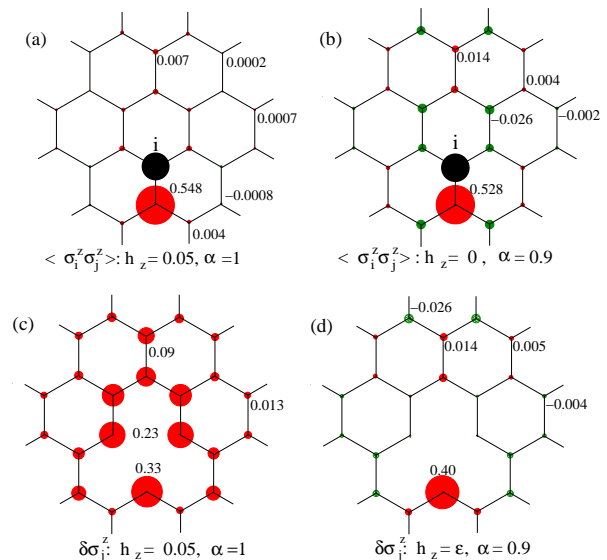


FIG. 6: (color online) (a, b) Correlation functions  $\langle \sigma_i^z \sigma_j^z \rangle$  with respect to site  $i$  indicated by a black circle. (c, d) Induced magnetization patterns  $\delta \sigma_j^z$  due to the presence of a vacancy, on the  $N = 24$  cluster. Circle areas are proportional to the quantities shown. Parameters are respectively  $(\alpha, h_z) = (1, 0.05)$  in (a) and (c), while  $(\alpha, h_z) = (0.9, 0)$  in (b) and (d) [a small symmetry-breaking field  $h_z = \epsilon = 5 \cdot 10^{-4}$  was added in (d)].

magnetization:

$$\delta \sigma_j^z = \langle \sigma_j^z \rangle - m_0,$$

which gives, for a given field  $h_z$  and site  $j$ , the change of the magnetization at this site relative to its value ( $m_0$ ) in the vacancy-free system. We relate the vacancy-induced magnetization pattern to the correlation function  $\langle \sigma_i^z \sigma_j^z \rangle$  of the vacancy-free system. The most striking feature of the magnetization patterns shown in Fig. 6(c,d) is the large magnetization on the  $z$ -neighbor of the vacancy (referred to as site  $k$  in Fig. 7 from now on). The magnetization is significantly larger there than on any other site – and only on this site does it remain finite at vanishing field in the Kitaev model:  $\langle \sigma_j^z \rangle \rightarrow \delta_{j,k} m_N$  for  $\alpha = 1$  and  $h_z \rightarrow 0$  ( $m_N \simeq 0.48$  for  $N = 24$ ). Actually, in the thermodynamic limit (TL) the magnetization (both the total one and  $\langle \sigma_k^z \rangle$ ) should behave with field as<sup>15</sup>  $h_z \ln(h_z)$ ; our results are consistent with this prediction in the sense that  $m_N$  decreases with increasing  $N$ , so that it should vanish in the TL as expected. As for the logarithmic field-dependence, we stress that this feature pertains to the TL, while for finite systems we can only notice weak non-linearities in the magnetization curves, discussed later in more detail.

The magnetic response localized on the  $z$ -neighbor of the vacancy is clearly connected with the fact that the correlation function  $\langle \sigma_i^z \sigma_j^z \rangle$  is non-zero only between nearest-neighbors sharing a  $z$ -bond<sup>11,14</sup>: if one spin is removed at site  $v$ , the term  $\sigma_v^z \sigma_k^z$  obviously disappears

from the Hamiltonian and thus the spin  $k$  is easily polarizable by the  $z$ -oriented field (one can also interpret this behavior in terms of dangling Majorana fermions<sup>15</sup>).

Yet, we already saw in Section II A that a small field induces  $\langle \sigma_i^z \sigma_j^z \rangle$  correlations beyond nearest neighbors, it makes sense to focus in more detail on the magnetization pattern around a vacancy at small finite  $h_z$ . Fig. 6(c) shows the variation of magnetization  $\delta\sigma_j^z$  due to the presence of the vacancy. Indeed, the spatial variations of this quantity presents similarities with those of correlations in the vacancy-free system:  $\delta\sigma_j^z$  is positive everywhere and decreases with increasing distance to the vacancy. Moreover, the spatial oscillations of correlation function appear in the magnetization pattern. Indeed, if one compares values of  $\delta\sigma_j^z$  at relative position either  $\vec{n}_1 + \vec{n}_2$  or  $2\vec{n}_1 - \vec{n}_2$  from the vacancy [see values 0.09 and 0.013 respectively in Fig. 6(c)], their respective ratio is comparable to that of corresponding correlations in the vacancy-free system.

While  $\langle \sigma_j^z \sigma_i^z \rangle$  correlations scale as  $h_z^2$ , the magnetization enhancement  $\delta\sigma_j^z$  on further neighbors of the vacancy grows approximately linearly with  $h_z$ ; in contrast, for  $j = k$ , it decreases from  $m_N$  at  $h = 0$  towards small negative values in the polarized phase (see  $\delta\sigma_k^z$  in Fig. 7). Although the response observed here is obtained for a finite cluster size, we may expect that in a large system, the spin at site  $k$  acquires a large magnetization due to the combined effect of the neighboring vacancy and the small field, and in turn polarizes its other neighbors in a way that the  $\delta\sigma_j^z$  reproduces the above discussed correlation function pattern (Fig. 6(a)).

If one considers the effect of a vacancy on the magnetic response of the system in a field  $h_z$ , a relevant quantity to consider is  $\delta M^z(h_z) = M^z[N-1, h_z] - (N-1)m_0(h_z)$ , with  $m_0$  the magnetization *per site* of the vacancy-free system, and  $M^z[N-1, h_z]$  is the total magnetization of the system with  $N-1$  spins plus a vacant site.

This quantity, shown in Fig. 7, vanishes in the infinite field limit (where all spins are polarized), but also at small field in the TL. In finite systems, the previously discussed finiteness of  $m_N$  goes along with a deviation from the expected logarithmic behavior of  $M^z$ ; yet, we notice on large enough systems ( $N = 24$ ) a non-linearity of the magnetization curve in the small field range  $h_z \ll h_{L/F}$ , the slope  $\frac{d(\delta M^z)}{dh_z}$  decreasing moderately with increasing small  $h_z$ . But when  $h_z$  becomes close to the value  $h_{L/F}$  of the liquid/polarized transition for the undoped system, the slope  $\frac{d(\delta M^z)}{dh_z}$  increases strongly, so that  $\delta M^z$  peaks near  $h_z \simeq 0.12(2)$ . The exact position of the peak depends slightly on the cluster size, and the peak amplitude grows with increasing system size (roughly linearly: compare amplitudes for  $N = 16$  and  $N = 24$  on Fig. 7). The existence of this peak can be understood in the following way: not only does the presence of a vacancy cause an increase of the magnetization in the liquid phase, but it shifts slightly the liquid/polarized transition towards

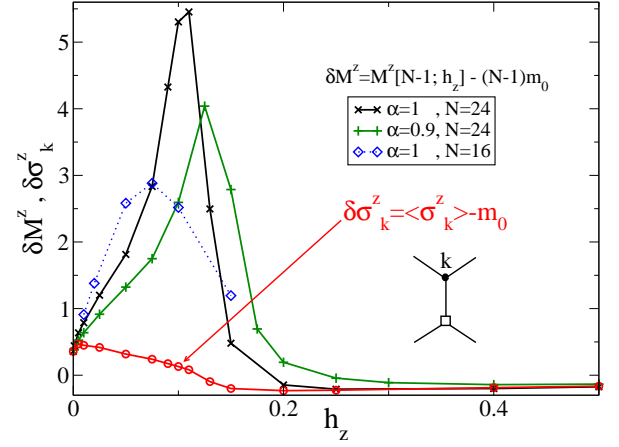


FIG. 7: Spin-vacancy induced magnetization  $\delta M^z$  as a function of magnetic field  $h_z$ , for different  $\alpha$  and cluster sizes. Shown also is a partial contribution (open circles) of the spin at site  $k$ , being the  $z$ -neighbor of the vacancy, for  $\alpha = 1$  and  $N = 24$ .

smaller fields  $h'_{L/F} < h_{L/F}$  (the difference between both fields being likely proportional to the vacancy concentration in a diluted limit), and the peak signals a field range  $h'_{L/F} < h_z < h_{L/F}$ . This behavior can loosely remind of spin polarons formed around mobile holes in a paramagnetic background, so that the temperature of transition to the ferromagnetic (FM) phase shifts up with increasing hole density<sup>35</sup>. Here, instead of temperature the parameter driving the transition is the magnetic field, and moreover a vacancy is here not mobile, but its effect is as well to polarize its surroundings more and more when approaching the FM phase; consequently, at small finite vacancy concentration, the transition field should be slightly smaller than in the vacancy-free case.

An analogy between the spin correlations in the vacancy-free system and the magnetization pattern around a vacancy can also be noticed in the case where the Kitaev Hamiltonian is perturbed by small Heisenberg interactions [see Fig. 6(b) and Fig. 6(d)]. Note that in Fig. 6(d), we also included an infinitesimal field  $h_z$ , the effect of which is only to break the Kramers degeneracy related to the odd number of spins. There, both the correlations and the vacancy-enhanced magnetizations  $\delta\sigma_j^z$  decrease rapidly with distance to the vacancy. Moreover the sign of these quantities alternates consistently with the pattern of  $z$ -oriented stripes shown in inset of Fig. 8, and their decrease is much faster when going perpendicularly to stripes than along stripes: for the magnetizations  $\langle \sigma_j^z \rangle$  (or equivalently  $\delta\sigma_j^z$ , since  $m_0 \simeq 0$ ), one can again compare in Fig. 6(d) the absolute values at positions  $2\vec{n}_1 - \vec{n}_2$  (0.004) and  $\vec{n}_1 + \vec{n}_2$  (0.014) from the vacancy.

The staggered  $z$ -bond magnetization, which measures

the  $z$ -stripe order parameter,

$$m^z(\vec{Q}_z) = \frac{1}{N} \sum_{\vec{r}} e^{i\vec{Q}_z \cdot \vec{r}} \langle \sigma_{\vec{r},A}^z + \sigma_{\vec{r},B}^z \rangle, \quad (10)$$

is shown in Fig. 8. It also evidences that, in the liquid phase, the short-range stripe pattern is induced around the vacancy by small Heisenberg interactions. Starting from the  $\alpha = 1$  limit, the magnetizations at further neighbors increase (in absolute values) significantly with increasing amplitude of Heisenberg interactions, i.e. with decreasing  $\alpha$ . We expect that the extensive quantity  $Nm^z(\vec{Q}_z)$  diverges in the TL for  $\alpha \rightarrow \alpha_{S/L}$ . Moreover, we note that the vacancy-induced magnetization  $\delta M^z$ , for fixed small field  $h_z$ , is reduced by the presence of Heisenberg interactions. It is significantly smaller for  $\alpha = 0.9$  than for  $\alpha = 1$ , as the tendency to stripe order around the vacancy, at small field, competes with the aligning effect of the field. Consequently, the peak in  $\delta M^z(h_z)$  shifts slightly towards higher fields with decreasing  $\alpha$ : the effect of Heisenberg interactions is to increase the position  $h'_{L/F}$  of transition to the polarized phase (as for  $h_{L/F}$  in the vacancy-free case, see Fig. 3).

We briefly comment here on the fact that in the polarized phase (and unlike in small field), the vacancy-induced magnetization change  $\delta\sigma_k^z$  at the  $z$ -neighbor is negative. This can be understood with the perturbative treatment of transverse interactions described in Section II A; but here, to evaluate the quantum correction to the magnetization at a given site, we consider the off-diagonal (perturbing) couplings only on neighboring bonds – see Ref. 36 for a similar approach. Within this approach, the magnetization at this site is  $\langle \sigma_k^z \rangle \simeq 1 - \frac{\alpha^2}{(h_z + 2\alpha - 1)^2}$ ; and the predicted value for  $\delta\sigma_k^z$  is of the same order as seen in Fig. 7 and it decreases in a similar way as  $h_z$  increases, sufficiently far away from the transition field to either the liquid or the stripe phase. Qualitatively, one can interpret this by the fact that at high field, fluctuations from a fully-polarized state are effectively stronger at the vacancy's  $z$ -neighbor than elsewhere, since the absence of ferromagnetic interaction on the missing  $z$ -bond makes it easier to flip this spin than other spins. With a similar reasoning one can explain that, in the same field range, the magnetization at other nearest neighbors of the impurity is enhanced compared to  $m_0$ .

If, instead of a field along an easy axis, a field in the  $[111]$  direction is applied, one can assume<sup>15</sup> that the magnetic response is approximately a linear combination of responses to each field component: thus each neighbor of a vacancy acquires an anomalously large magnetization – the neighbor spin at site  $j$ , that would be connected to the missing spin by a  $\gamma$ -bond, has a magnetization  $\langle \sigma_j^z \rangle \sim h_\gamma \ln(h_\gamma)$ , and in turn brings a smaller polarization, also parallel to  $h_\gamma$ , to other spins in its vicinity – mainly on neighboring sites which are close to the spatial axis in the prolongation of the missing  $\gamma$ -bond. Hence, three domains should coexist in the system, each with a different magnetization direction. Note that a vector

$\vec{m}_{stripe} = [m^x(\vec{Q}_x), m^y(\vec{Q}_y), m^z(\vec{Q}_z)]$  can be defined and used to characterize the polarization of spins around the vacancy. Qualitatively,  $\vec{m}_{stripe}$  should point in a direction closer to the easy axis  $\gamma$  for which  $h_\gamma$  is the largest than to other easy axes; but it can have three non-zero components simultaneously.

## B. Stripe orientation in a small field and anisotropy of magnetic response

In the stripe-ordered phase, among the 6 allowed stripe patterns (3 possible stripe directions times 2 spin orientations), a vacancy in combination with an infinitesimal field  $h_z > 0$  selects the  $z$ -stripe pattern for which  $M^z = 1$  up to small quantum corrections. This selection is due to the necessary imbalance between the number of spins respectively aligned and antialigned with the field (see inset of Fig. 8). This state is stable versus increasing  $h_z$ , until the field reaches a critical value (or anisotropy field  $h_{an}$ ), where canted stripe patterns – those with stripe directions along  $x$  or  $y$  – become more favorable. This effect is similar to the local rotation of the staggered magnetization close to a vacancy in  $SU(2)$  antiferromagnets<sup>22</sup>. Here, the main difference is that there is only a finite number of stripe patterns which cannot be continuously connected to each other without going out of the ground state manifold; consequently, the system has to choose between allowed stripe patterns, tilted or not by the field, and  $\vec{m}_{stripe}$  is forced to point exactly along one easy axis  $\gamma$ , corresponding to (one of) the most favorable pattern(s). To understand the existence of a finite anisotropy field, one has to compare the energy of the  $z$ -stripe pattern (*untiltable*<sup>30</sup> in a  $[001]$ -field) to that of the *tiltable*  $x$ - and  $y$ -stripe patterns. The former, thanks to its total magnetization  $M^z \simeq +1$ , acquires locally an energy gain  $\simeq -h_z$  with respect to the zero-field value but it has zero susceptibility ( $\chi^z = 0$ ) thus no contribution  $\propto Nh_z^2$  to its energy; in contrary, the field lowers the energy of the latter patterns by an extensive quantity  $\delta E \simeq -(N-1)\frac{h_z^2}{8(1-\alpha)}$ . This comparison gives  $h_{an} = 8\frac{1-\alpha}{N-1} \simeq 0.10$  for  $\alpha = 0.7$ , not far from the position of the jump in  $M^z(h_z)$  in Fig. 8.

In the vicinity of the stripe-liquid transition, the magnetization pattern induced by a small  $[001]$ -field ( $|h_z| \ll 0.1$ ) around a vacancy can be of special interest: assuming that vacancies are diluted enough such that their mutual interactions can be neglected, the patterns expected on both sides of the transition are clearly distinct from each other. In the stripe phase, all neighboring spins of the vacancy have a large, almost field-independent magnetization, with two of them aligned with the field and the third one antialigned with  $\vec{h}$ . In contrast, in the liquid phase only one nearest neighbor spin is significantly polarized (with a strongly field-dependent polarization) and aligned with the field; and the two others are weakly polarized opposite to the field. Thus, if one would have



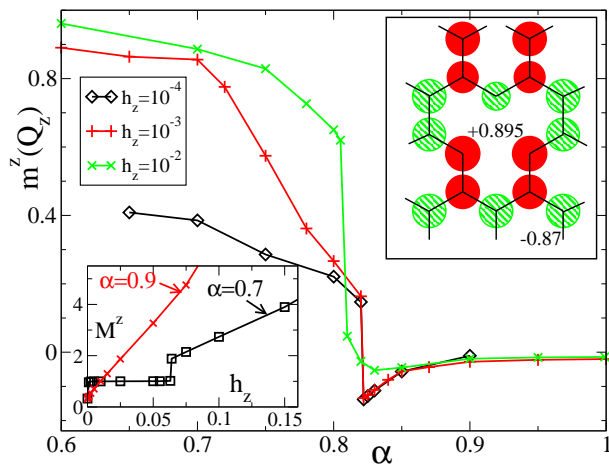


FIG. 8: (color online) The  $z$ -stripe order parameter  $m^z(\vec{Q}_z)$  computed on the  $N = 24$  cluster, as a function of  $\alpha$  at different small fields  $h_z$ . Right-inset: The magnetization pattern  $\langle \sigma_r^z \rangle$  around the vacancy for  $\alpha = 0.7$  and  $h_z = 10^{-3}$ . Left-inset: Total magnetization  $M^z$  as a function of a field  $h_z$  applied in the liquid ( $\alpha = 0.9$ ) and in the stripe ( $\alpha = 0.7$ ) phases, with a magnetization jump at  $h_{an} \simeq 0.062$ .

a local probe to determine the (site-resolved) magnetization in the neighborhood of a vacancy – this probe could be  $^{23}\text{Na}$  NMR for instance – the measured pattern could indicate on which side of the transition the system is.

We have also seen that a vacancy can block the spin canting mechanism in the stripe phase, under a small field in (or close to) the  $[001]$  axis. This phenomenon is absent for a field in the  $[111]$  direction, where all stripe patterns remain equivalent and continuously tiltable by the field. Consequently, in a finite system, the situation concerning the susceptibility anisotropy at zero-field:  $\chi^z = 0 < \chi^{[111]}$ , is now opposite to the previously discussed case without vacancies where we found  $\chi^{[111]} < \chi^z$ . Concerning now the thermodynamic limit with a finite concentration  $n_v$  of vacancies, if one assumes that  $n_v$  is large enough to influence the magnetic response at low temperatures but small enough so that vacancies behave independently from each other, a similar effect could account for the experimentally observed  $\chi^{ab} < \chi^c$ . However, given that in a small field, within the Kitaev model, the magnetization enhancement caused by two vacancies residing on the same sublattice is much larger than twice the magnetization enhancement caused by a single vacancy<sup>15</sup>, one should take care about cooperative effects between the vacancies.

#### IV. INTERACTION BETWEEN VACANCIES: BROKEN ORIENTATIONAL SYMMETRY AND MAGNETIZATION PROPERTIES

We turn now to the case where several vacancies are present in the system; we first consider their effect on

the magnetization curves; then, we will focus on their effective interaction in the stripe phase and show how a vacancy pair can select an ordered pattern.

##### A. Comparison of magnetic response with vacancy pairs in various phases

It is instructive to compare the effect of vacancies or pairs of vacancies on magnetization curves, for given field direction and system size. To do this comparison we choose a  $[001]$ -field and consider the periodic  $N = 24$  cluster, but discuss as well implications for the thermodynamic limit. Magnetization curves  $M^z(h_z)$  with or without vacancies, in different phases of the Kitaev-Heisenberg model, are shown in Fig. 9.

*In the Néel phase*, although the total magnetization  $M^z = \sum_i \langle \sigma_i^z \rangle$  is not a conserved quantity in presence of small Kitaev interactions ( $\alpha \ll \alpha_{N/S}$ ), the magnetization curve  $M^z(h_z)$  on finite clusters displays a succession of plateaux (almost flat for  $\alpha = 0.1$ ), as seen in Fig. 9(a). They are separated by jumps  $\Delta(M^z) \simeq +2$  corresponding to a flip of one spin  $1/2$ . At fixed  $\alpha$  the step-like increase of the magnetization per site  $m_0(h_z)$  disappears only in the TL, the steps becoming smaller and closer to each other as  $N$  increases. Moreover the steps disappear, at fixed cluster size, as  $\alpha$  gets closer to  $\alpha_{N/S}$ .

Within this phase, one is tempted to define an effective spin  $1/2$ ,  $\tilde{S}_{eff}$ , associated to the vacancy, such that  $M^z(h_z \rightarrow 0) = +1$  corresponds to  $\tilde{S}_{eff}$  pointing along  $+z$ ; with two vacancies, their effective  $\tilde{S}_{eff}^z$ 's add up if vacancies are on the same sublattice (e.g., n.n.n. case) and cancel each other if on opposite sublattices (n.n. case). From the behavior of  $M^x(h_x \rightarrow 0)$  one obtains similar conclusions concerning effective couplings between other components of  $\tilde{S}_{eff}$ . One could therefore think that an effective interaction between two vacancy spins, if it can be defined, should be  $SU(2)$ -invariant, and possibly of Heisenberg type  $\tilde{S}_{eff}^i \cdot \tilde{S}_{eff}^j$ ; yet, the gapless nature of the undoped system and the continuous behaviour of magnetization curves in the TL make it unclear how to formulate the effect of vacancies in terms of effective spins.

*In the liquid phase*, in contrast, the magnetization does not show any plateau, but vacancies cause peculiar features at small fields: We have already seen that, compared to the zero-vacancy curve, the slope of  $M^z(h_z)$  at small field is significantly increased by the presence of one vacancy in the system. If two vacancies are present, their effect depends strongly on their respective sublattices (see Fig. 9(c)): if they are on opposite sublattices the  $M^z(h_z)$  curve is, as in the vacancy-free case, linear for small  $h_z$  [and  $\chi^z(h_z \rightarrow 0)$  is only slightly modified]; but if they are on the same sublattice, this slope is greatly increased – for a large range of  $h_z$  the vacancy-induced increase in  $M^z$  is more than twice that of the single-impurity case. Again, even though we cannot identify a logarithmic behavior  $\chi^z(h_z) \sim 1/(h_z \ln^{3/2} h_z)$  as derived

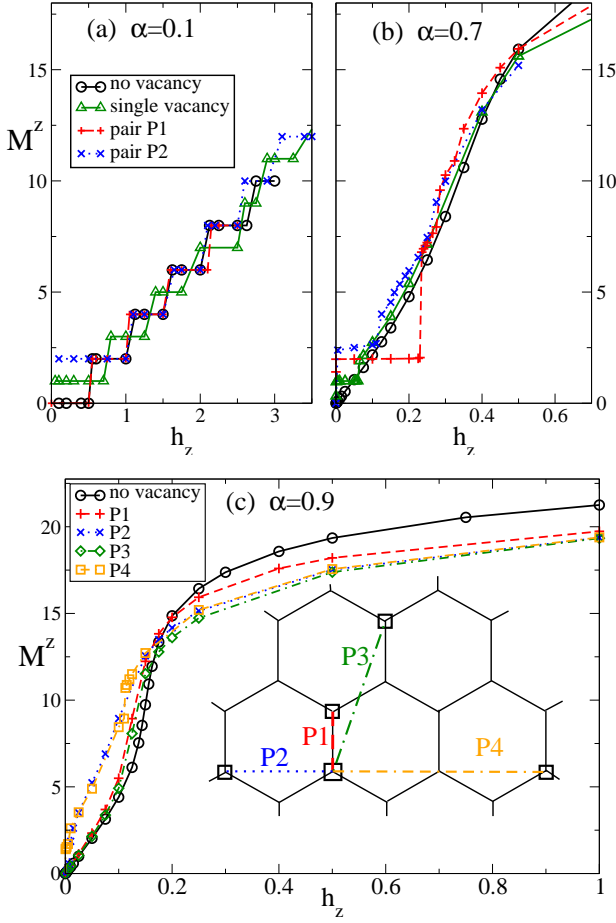


FIG. 9: (color online) Magnetization curves  $M^z(h_z)$  on the cluster  $N = 24$  with 0, 1, or 2 vacancies. The labels  $P1, \dots, P4$  correspond to relative positions of 2 vacancies as shown in panel (c). Panels (a),(b), and (c) correspond to  $\alpha = 0.1, 0.7, 0.9$ , respectively.

in Ref. 15 for  $\alpha = 1$ , we see that vacancies, as soon as they are not equally distributed on both sublattices, act like *partially-unbound moments* causing non-linearities in the magnetization properties at low field.

In the *stripe phase*, as in the liquid phase, Kitaev interactions are strong enough to prohibit the existence of plateaux in the magnetization curves  $M^z(h_z)$ , except at small fields in presence of vacancies: with one vacancy, the previously discussed  $M^z = 1$  plateau is again suggestive of an effective spin 1/2 of the vacancy; and with two vacancies on the same sublattice, the  $M^z \simeq 2$  plateau seen on Fig. 9(b) (pair P1) extends up to a field  $h_{an2} \leq 0.22(1)$ , that is more than twice the anisotropy field  $h_{an}$  for a single vacancy. This indicates a cooperative effect of both vacancies, which stabilize the  $z$ -stripe pattern more than if they behaved independently from each other. To describe this cooperative behavior, we will, similarly as in Section III B, analyze the effect of vacancies on the energies of the various stripe patterns.

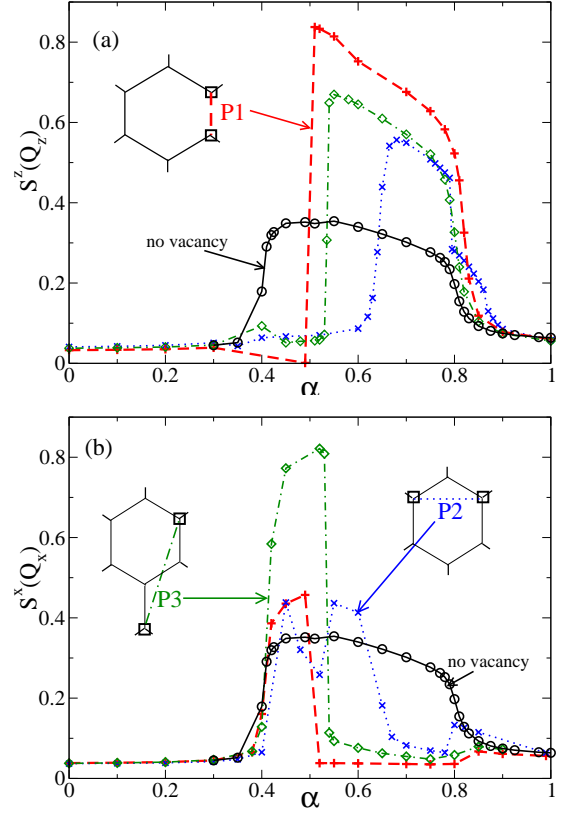


FIG. 10: (color online) Structure factors (a)  $S^z(\vec{Q}_z)$  and (b)  $S^x(\vec{Q}_x)$  at  $h = 0$  calculated for various respective positions of 2 vacancies  $P1, P2, P3$ , indicated in the insets. Also shown is the structure factor of the vacancy-free system (open circles), for which  $S^z(\vec{Q}_z) = S^x(\vec{Q}_x)$ . All results are obtained on the  $N = 24$  cluster.

## B. Selection of stripe orientation by vacancy pairs

We focus now on the stripe-ordered phase, and will explore how at  $h = 0$ , a pair of defects can, depending on their relative position, favor or disfavor one of the three stripe directions. In terms of symmetries, this can be understood as a breaking of  $\mathbb{Z}_3$  symmetry related to the spatial orientation of stripes, while the  $\mathbb{Z}_2$  symmetry ( $\vec{\sigma}_i \rightarrow -\vec{\sigma}_i$ ) remains unbroken. Remarkably, as shown in Fig. 10, the selected stripe pattern for a given vacancy pair depends on the coupling constant  $\alpha$ .

This effect is easy to understand for nearest-neighbor defects on a  $z$ -bond (configuration  $P1$ : see Fig.10); classically, the  $z$ -stripe pattern has an energy lower by

$$\delta E_1^z = 2 - 4\alpha \quad (11)$$

than the one of other stripe patterns. Indeed, in the  $z$ -pattern only one FM bond - here a  $z$ -bond, with a classical contribution to the energy  $1 - 3\alpha$  - is lost due to vacancies, instead of two for other patterns (e.g. two  $x$ -bonds, in a  $x$ -stripe pattern), and for  $\alpha > 0.5$  FM interactions contribute more than AF ones (whose classical

contribution to the energy is  $\alpha - 1$ ). For  $\alpha < 0.5$  the situation is reversed, which explains that  $S^z(\vec{Q}_z)$  becomes small and  $S^x(\vec{Q}_x) = S^y(\vec{Q}_y) \simeq 1/2$ .

For second neighbors (case *P2* on Fig. 10), stripe patterns are classically degenerate, but this degeneracy is lifted by quantum fluctuations. We evaluate in second order perturbation theory the contribution to the energy of various bonds in which at least one site is a neighbor of the vacancy; actually only AF bonds give a contribution in this approximation. For instance fluctuations on a bond belonging to the same hexagon as the two impurities yield a contribution  $-4(1-2\alpha)^2/[4(1-\alpha)+2(3\alpha-1)]$  to the energy of the  $z$ -stripe state. Collecting contributions from all relevant bonds, the energy of the  $z$ -stripe state (relative to that of other stripe orientations) is:

$$\delta E_2^z = 2(1-2\alpha)^2 \left( \frac{1}{5\alpha-1} + \frac{1}{2\alpha} - \frac{2}{1+\alpha} \right), \quad (12)$$

which is positive for  $\alpha$  in the vicinity of  $1/2$ , and changes sign at  $\alpha_2 \simeq 0.651$ . This explains the drop of the  $z$ -stripe structure factor (dotted curve on Fig. 10(a)), from large values for  $\alpha \in [0.64(2); 0.8]$ , to almost zero for smaller  $\alpha$ . The smaller values of  $S^x(\vec{Q}_x) \simeq 0.3$  in the vicinity of  $\alpha = 0.5$  are related to the smaller energy scale separating the different stripe patterns: the above expression, with its prefactor  $(1-2\alpha)^2$ , indicates that the 3 patterns become degenerate at  $\alpha = 0.5$ .

A similar energy comparison between different patterns for third neighbor vacancy pairs (configuration *P3*: see Fig. 10) predicts a change of stripe orientation at  $\alpha_3 = 0.6$  between  $z$ -stripes ( $\alpha_3 < \alpha < \alpha_{LS}$ ) and  $x$ -stripes ( $\alpha_{SN} < \alpha < \alpha_3$ ), following from the perturbative result:

$$\delta E_3^z = \frac{(1-2\alpha)^2(3-5\alpha)}{1-\alpha^2}, \quad (13)$$

whereas this orientational change is seen on  $N = 24$  at a slightly smaller value  $\alpha_3 \simeq 0.53(1)$ . Notice that here (and more generally for pairs of vacancies at further neighbor sites which are not related to each other by any reflection symmetry of the honeycomb lattice) the three stripe orientations are all non-equivalent to each other.

Finally we note that at zero-field, the conclusions above hold also for pairs of neighbor vacancies with other relative positions: for instance with next-nearest neighbor vacancies separated by a  $x$ - and a  $z$ -bond and  $\alpha > \alpha_2$ , according to the previous reasoning the favored pattern is a  $y$ -stripe pattern.

In presence of a small magnetic field, the  $\mathbb{Z}_2$  symmetry characterizing each stripe orientation (e.g.,  $z$ -stripes) is broken. Moreover, similar effects occur as in the previously discussed single vacancy case: if the most favorable pattern in an infinitesimal  $[001]$  field (e.g.,  $z$ -stripe pattern around a vacancy pair in configuration *P1*, for  $\alpha > 0.5$ ) is untiltable for this field direction, as the field amplitude  $h_z$  gets larger than a critical value  $h_{an2}$  this pattern becomes less favorable than other patterns which

are tiltable. In the limit of large systems  $N \gg 1$ , a classical estimate of  $h_{an2}$  gives a result  $4(2\alpha-1)(1-\alpha)/\sqrt{N}$  which, for  $\alpha = 0.7$  and  $N = 24$ , has a value  $h_{an2} \simeq 0.28$  comparable to the observed position of the magnetization jump.

The relevant quantity for the discussion of either low temperature properties or magnetic ordering at small vacancy concentrations is the energy scale  $\delta E_n^z$ , namely the energy which favors a particular stripe pattern in the vicinity of a vacancy pair –  $n$  standing for the number of bonds separating both vacancies. Far away from the stripe/liquid transition (say, for  $\alpha \leq 0.7$ )  $\delta E_n^z$  decreases rapidly with  $n$  (e.g.,  $|\delta E_n^z| \leq |\delta E_1^z|/2$  for  $n \geq 2$ ). Closer to  $\alpha_{S/L}$ , larger quantum fluctuations make the stripe-orientation selection by  $3^{rd}$  neighbor vacancy pairs as efficient as by nearest neighbor vacancy pairs.

Several consequences can result from this: (i) In the simpler case with only two vacancies, the energy lowering of some stripe patterns for  $\alpha \simeq \alpha_{S/L}$  also stabilizes these patterns with respect to the spin liquid, which leads to a slight shift of the stripe/liquid transition towards larger  $\alpha$  – possibly 0.82 to 0.85 depending on the relative position of vacancies, as can be seen in Fig. 10(a). (ii) More importantly, if one focuses on systems with substantial vacancy concentrations, say,  $n_v \sim 10\%$ , neighboring vacancy pairs as described in Fig. 10 are abundant enough to select locally stripe orientations that will frustrate each other at the global scale. (iii) As a result, the system could display a glassy behavior, especially in the vicinity of the stripe-liquid transition. The resulting glassy phase would consist of stripe-ordered nanoscale domains, with a vacancy pair in each domain, selecting its stripe orientation. In order to perform a modeling of such a system and to reproduce a possible spin-glass behavior, one should obviously need to consider systems of (at least) hundreds of Ir atoms, and to take into account the energy cost of domain walls between regions of different stripe orientations. Moreover, obviously not all vacancies are grouped into distinct first, second or third nearest neighbor vacancy pairs; in particular the effect of unpaired vacancies, even at zero external field, could be subtle, although one can imagine single vacancies pinning walls between domains of different stripe orientation.

## V. SUMMARY AND CONCLUDING REMARKS

We have considered here several important aspects of the Kitaev-Heisenberg model, which, despite its simple structure, displays in its  $T = 0$  phase diagram three distinct phases, two of which are antiferromagnetically ordered while the third one is a spin liquid. We employed numerical methods (exact diagonalization) for our investigation of the properties of the model in a magnetic field and the effect of vacancies on the magnetic properties. The numerical methods were complemented by classical and perturbative analysis particularly in the frame of the

stripe phase.

We showed how the ground state phases evolve in a magnetic field oriented along the [001] direction (one of the local easy axes of the Kitaev-Heisenberg Hamiltonian). We found that the three phases are robust to small fields. Next, we analyzed the influence of the field direction. The magnetic response is qualitatively distinct in the different phases. In the stripe phase, the magnetization can be described by a spin canting mechanism, which also provides an understanding of the anisotropy in the numerically obtained susceptibilities. In the liquid phase, we compared the effect of small magnetic fields and of small Heisenberg interactions, each considered as a perturbation of the Kitaev Hamiltonian. Such perturbations are shown to induce specific patterns in the spin-spin correlations beyond nearest neighbors, while at larger fields a transition into the spin-polarized phase occurs. We determined the phase diagram of the model in a [001]-field, with good agreement between numerical results and analytical estimates. For the latter analysis, we took into account both the spin canting and the quantum fluctuations in the ordered and polarized phases. This phase diagram has similarities with its counterpart for a [111] field orientation<sup>28</sup>, however, a major difference between them is that for a [001]-field we do not see any quantum critical point in the vicinity of the stripe-liquid phase transition. We presume that this is related to the absence of a field-induced gap in the low-energy spectrum of the liquid phase for a [001]-field<sup>11</sup>.

Subsequently, we focused on the effect of non-magnetic vacancies on the spin correlations and the magnetic response of the model. For a single vacancy in the liquid phase, we found that the spatially anisotropic magnetization pattern around the vacancy is related to the anisotropy of spin correlations in the vacancy-free system. Up to finite-size effects inherent to our approach, these results are also in agreement with predictions of a non-linear response to a small [001]-field, whose effect is mostly seen on one specific neighbor of the vacancy. In the stripe phase, a vacancy coupled to a small [001]-field breaks both the  $\mathbb{Z}_2$  (time reversal) and the  $\mathbb{Z}_3$  (orientational) symmetry characterizing the ground state manifold; a single stripe pattern is selected, which is not continuously tiltable by the field in contrast to the vacancy-free situation.

Having in mind the description of systems at finite vacancy concentration, we considered the interplay of two vacancies sitting either on nearest or further neighbor sites. Again the magnetic response to an easy-axis field depends strongly on the nature of the phase, but it also depends sensitively on the relative position of vacancies. In the liquid phase a non-linear behavior, much stronger than for the single-impurity case, is seen if the two vacancies are on the same sublattice, while the response remains linear if they reside on different sublattices. In the stripe phase, vacancy pairs select a specific stripe orientation even at zero field. This selection mechanism, depending on the value of coupling parameter  $\alpha$ , can be well

understood by a perturbative approach evaluating locally the effect of quantum fluctuations. The response to a small field depends on whether the selected stripe pattern is tiltable or not for this field direction<sup>30</sup>. Although the strongest selection effect is caused by nearest neighbor vacancy pairs for a wide range of  $\alpha$ , further neighbor pairs have to be considered as well in the vicinity of the stripe-liquid transition. Therefore we conclude that the intrinsic randomness of vacancies, in combination with the selection mechanism induced by vacancy pairs, may lead to spin-glass behavior in the stripe regime. There, a vacancy concentration of a few percents should be enough for the system to show a glassy behavior, with a tendency to the formation of stripe-ordered nanodomains around vacancy pairs.

Finally, we comment on the possible relevance of this work to layered iridates, which motivated the derivation of the Kitaev-Heisenberg model. The experimental data (magnetic susceptibility, heat capacity<sup>19,20</sup>) on  $\text{Na}_2\text{IrO}_3$  indicate antiferromagnetism at low temperature and a substantial magnetic anisotropy. Yet, the angular dependence of the measured susceptibility is qualitatively opposite to that found for a vacancy-free model. We then showed that non-magnetic vacancies in the dilute limit, i.e., where interactions between vacancies are irrelevant, can reverse locally this tendency by blocking the spin-canting for some field directions. The recent x-ray magnetic scattering data<sup>21</sup> ruled out the Néel state, implying that the Kitaev interaction in  $\text{Na}_2\text{IrO}_3$  may dominate over a simple Heisenberg coupling. In addition to the stripe phase intrinsic to the Kitaev-Heisenberg model, the so-called "zig-zag" spin order is also consistent with the data<sup>21</sup>. An element in favor of a description of layered iridates  $\text{A}_2\text{IrO}_3$  ( $\text{A}=\text{Li}, \text{Na}$ ) by the Kitaev-Heisenberg model is the comparison of the low temperature susceptibilities of these compounds<sup>32</sup>. Using our result  $\chi \propto \frac{1}{1-\alpha}$  for the stripe phase, we found a relation between  $\alpha$  values in these two compounds, which indicates that the Li compound, as the Na-based one, is most probably in the stripe phase but much closer to the transition towards the spin liquid. This conclusion is in agreement with previous work<sup>32,33</sup> estimating the relative  $\alpha$  values from a comparison of the paramagnetic Curie temperatures. The application of uniaxial pressure on a single crystal of  $\text{Li}_2\text{IrO}_3$  might even drive the system into the liquid phase.

To describe the experimental situation in layered iridates on a quantitative level, other factors such as lattice distortions have to be considered as well. In particular, the lattice distortions may bring about substantial anisotropy in the ground state  $g$ -factors and in the Van Vleck contribution to the magnetic susceptibility, originating from transitions to higher lying spin-orbital quartet split by non-cubic (tetragonal and/or trigonal) crystal fields. Furthermore, these distortions may lead to spin interactions not included in the Kitaev-Heisenberg model. For intermediate strength of spin-orbit coupling like in iridates, these effects might be essential for a quantita-



tive description of magnetic properties. Moreover, our study suggests that a glassy behavior could occur in the vicinity of the spin liquid phase; in this context, considering the present model at larger scales, with a finite density of vacancies, could help to explore the effect of temperature.

## Acknowledgments

The authors are indebted to R. Moessner and G. Jackeli for fruitful discussions at different stages of this work.

- 
- <sup>1</sup> P.A. Lee, *Science* **321**, 1306 (2008).
  - <sup>2</sup> L. Balents, *Nature (London)* **464**, 199 (2010).
  - <sup>3</sup> Y. Shimizu, K. Miyagawa, K. Kanoda, M. Maesato, and G. Saito, *Phys. Rev. Lett.* **91**, 107001 (2003).
  - <sup>4</sup> P. Mendels and F. Bert, *J. Phys. Soc. Jap.* **79**, 1 (2010).
  - <sup>5</sup> Y. Okamoto, M. Nohara, H. Aruga-Katori, and H. Takagi, *Phys. Rev. Lett.* **99**, 137207 (2007).
  - <sup>6</sup> S. Yamashita, *Nature Physics* **4**, 459 (2008).
  - <sup>7</sup> H.Y. Yang, A.M. Läuchli, F. Mila, and K.P. Schmidt, *Phys. Rev. Lett.* **105**, 267204 (2010).
  - <sup>8</sup> L.F. Tocchio, A. Parola, C. Gros, and F. Becca, *Phys. Rev. B* **80**, 064419 (2009).
  - <sup>9</sup> A. Ralko, M. Ferrero, F. Becca, D. Ivanov, and F. Mila, *Phys. Rev. B* **71**, 224109 (2005).
  - <sup>10</sup> Z.Y. Meng, T.C. Lang, S. Wessel, F.F. Assaad, A. Muramatsu, *Nature* **464**, 847 (2010).
  - <sup>11</sup> A.Yu. Kitaev, *Ann. Phys.* **321**, 2 (2006).
  - <sup>12</sup> S. Mandal and N. Surendran, *Phys. Rev. B* **79**, 024426 (2009).
  - <sup>13</sup> K. Dhochak, R. Shankar, and V. Tripathi, *Phys. Rev. Lett.* **105**, 117201 (2010).
  - <sup>14</sup> G. Baskaran, S. Mandal, and R. Shankar, *Phys. Rev. Lett.* **98**, 247201 (2007).
  - <sup>15</sup> A.J. Willans, J.T. Chalker, and R. Moessner, *Phys. Rev. Lett.* **104**, 237203 (2010); A.J. Willans, J.T. Chalker, and R. Moessner, arXiv:1106.0732.
  - <sup>16</sup> K.S. Tikhonov, M.V. Feigel'man, and A.Yu. Kitaev, *Phys. Rev. Lett.* **106**, 067203 (2011).
  - <sup>17</sup> G. Jackeli and G. Khaliullin, *Phys. Rev. Lett.* **102**, 017205 (2009).
  - <sup>18</sup> J. Chaloupka, G. Jackeli, and G. Khaliullin, *Phys. Rev. Lett.* **105**, 027204 (2010).
  - <sup>19</sup> H. Takagi (private communication).
  - <sup>20</sup> Y. Singh and P. Gegenwart, *Phys. Rev. B* **82**, 064412 (2010).
  - <sup>21</sup> X. Liu, T. Berlijn, W.-G. Yin, W. Ku, A. Tsvelik, Y.-J. Kim, H. Gretarsson, Y. Singh, P. Gegenwart, and J.P. Hill, *Phys. Rev. B* **83**, 220403 (2011).
  - <sup>22</sup> S. Eggert, O.F. Syljuasen, F. Anfuso, and M. Andres, *Phys. Rev. Lett.* **99**, 097204 (2007).
  - <sup>23</sup> H. Alloul, J. Bobroff, M. Gabay, and P.J. Hirschfeld, *Rev. Mod. Phys.* **81**, 45 (2009).
  - <sup>24</sup> C. Lhuillier and G. Misguich, *Two-dimensional quantum antiferromagnets*, H. T. Diep editor, World-Scientific (2005).
  - <sup>25</sup> R.L. Doretto and M. Vojta, *Phys. Rev. B* **80**, 024411 (2009); D. Poilblanc and A. Ralko, *Phys. Rev. B* **82**, 174424 (2010).
  - <sup>26</sup> S. Sachdev, C. Buragohain, and M. Vojta, *Science* **286**, 2479 (1999); K.H. Höglund and A.W. Sandvik, *Phys. Rev. Lett.* **91**, 077204 (2003).
  - <sup>27</sup> N.W. Ashcroft and N.D. Mermin, *Solid State Physics* (Saunders College Publishing, Philadelphia, 1976).
  - <sup>28</sup> H.C. Jiang, Z.C. Gu, X.L. Qi, and S. Trebst, *Phys. Rev. B* **83**, 245104 (2011).
  - <sup>29</sup> S. Mandal, S. Bhattacharjee, K. Sengupta, R. Shankar, and G. Baskaran, arXiv:1101.1388.
  - <sup>30</sup> A stripe pattern satisfying the condition of non-collinearity with the field will be called *tiltable*, and in contrary a pattern where spins are collinear to the field will be called *untiltable*.
  - <sup>31</sup> A quantitative comparison of our calculated susceptibilities to those measured in Ref. 20 would include also the effect of temperature, especially as the measured anisotropy was also large in the paramagnetic phase.
  - <sup>32</sup> Y. Singh, S. Manni, and P. Gegenwart, arXiv:1106.0429.
  - <sup>33</sup> J. Reuther, R. Thomale, and S. Trebst, arXiv:1105.2005.
  - <sup>34</sup> S. Dommange, M. Mambrini, B. Normand, and F. Mila, *Phys. Rev. B* **68**, 224416 (2003).
  - <sup>35</sup> C.M. Varma, *Phys. Rev. B* **54**, 7328 (1996); P. Horsch, J. Jaklič, and F. Mack, *Phys. Rev. B* **59**, 14149 (1999).
  - <sup>36</sup> B. Schmidt, M. Bortz, S. Eggert, M. Fleischhauer, and D. Petrosyan, *Phys. Rev. A* **79**, 063634 (2009).